



# Aerosol-assisted preparation of N-doped hierarchical porous carbon spheres cathodes toward high-stable lithium-ion capacitors

Yinghong Xu<sup>1</sup>, Jiangmin Jiang<sup>1</sup>, Zhiwei Li<sup>1</sup>, Ziqian Yang<sup>1</sup>, Yadi Zhang<sup>1</sup>, Yufeng An<sup>1</sup>, Qi Zhu<sup>1</sup>, Hui Dou<sup>1</sup>, and Xiaogang Zhang<sup>1,\*</sup>

<sup>1</sup>Jiangsu Key Laboratory of Electrochemical Energy Storage Technologies, College of Material Science and Engineering, Nanjing University of Aeronautics and Astronautics, Nanjing 210016, People's Republic of China

**Received:** 16 April 2020

**Accepted:** 10 June 2020

**Published online:**  
16 June 2020

© Springer Science+Business Media, LLC, part of Springer Nature 2020

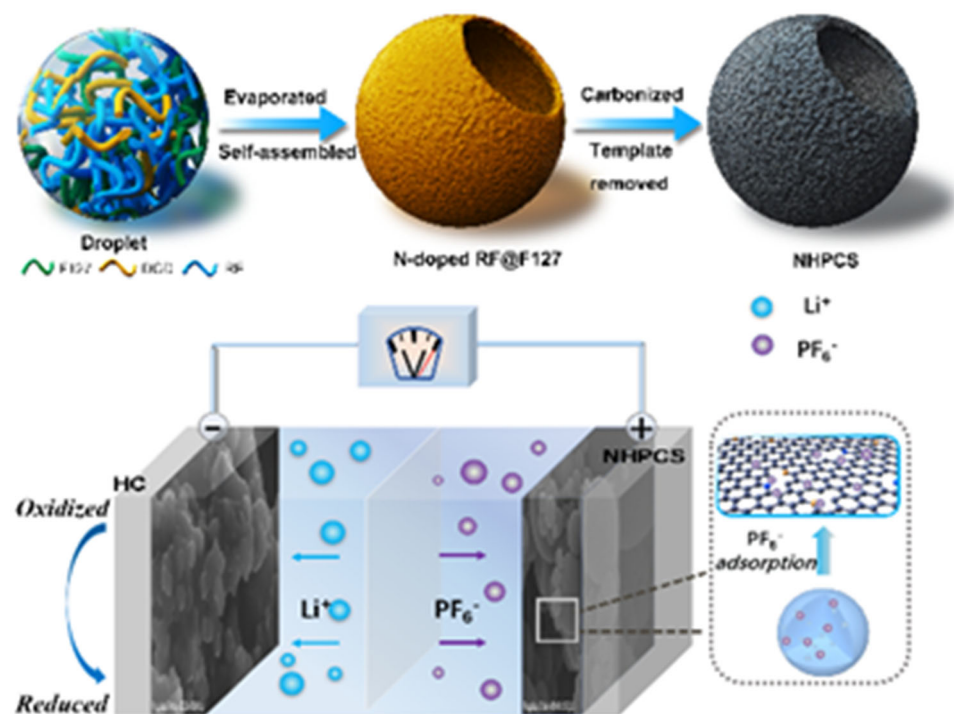
## ABSTRACT

Lithium-ion capacitors (LICs) are gradually emerging as one of the most indispensable hybrid energy storage devices. However, it is one main challenge to evade the mismatch of electrochemical kinetics and specific capacity between cathode and anode in LICs. Herein, we have proposed an efficient strategy to prepare the nitrogen-doped hierarchical porous carbon spheres (NHPCS) as cathode, which is synthesized by a simple aerosol-spraying pyrolysis using the low-cost phenolic resin as carbon source without any other catalyst or hard template. The NHPCS exhibits porous nanospheres structure with an appropriate nitrogen doping level (3.65 at.%). Benefitting from the two-pronged strategy of N-doped feature and nanostructure engineering, NHPCS achieves a high specific capacity of 74 mAh g<sup>-1</sup> at a current density of 0.1 A g<sup>-1</sup> and remains 86.5% of initial capacity even being subjected to a high rate of 50-fold. Furthermore, a high-performance LIC has been developed by coupling NHPCS cathode and hard carbon anode, which delivers a maximum energy density of 151 Wh kg<sup>-1</sup> and excellent cycle stability (96.3% capacity retention after 3000 cycles). Significantly, such designed porous carbon could not only be convenient for scalable production, but also be served for many other energy storage devices.

Address correspondence to E-mail: azhangxg@163.com

## GRAPHIC ABSTRACT

We have presented a larger-scale spray pyrolysis strategy to prepare nitrogen-doped hierarchical porous carbon spheres (NHPCS). A high-stable lithium-ion capacitor has been constructed by coupling NHPCS cathode with hard carbon anode, which exhibits a maximum energy density of  $151 \text{ Wh kg}^{-1}$  and capacity retention of 96.3% over 3000 cycles, showing great potential for the next-generation energy storage application.



## Introduction

In the context of the fossil energy exhaustion and the grim environmental problems, the development of renewable energy sources and new energy storage devices gradually becomes an imperative requirement in the future. As a new type of energy storage device, supercapacitors have been attracted wide attention because of their high power density and ultralong cycle life [1]. However, the relatively low energy density always limits their further developments and applications. Among various energy storage devices, lithium-ion capacitors (LICs) can output not only high power density but also satisfy

energy density, which combines the advantages of lithium-ion batteries (LIBs) and supercapacitors (SCs).

LICs are usually assembled with a capacitive cathode and a faradaic anode in a Li-ion-conducting organic electrolyte. Up to now, a series of electrode materials used for LICs have been reported. For instance,  $\text{Li}_3\text{VO}_4/\text{N-doped carbon}$  ( $529 \text{ mAh g}^{-1}$ ),  $\text{Li}_4\text{Ti}_5\text{O}_{12}$  ( $175 \text{ mAh g}^{-1}$ ), graphite ( $372 \text{ mAh g}^{-1}$ ), and other materials with high specific capacity were employed as anode electrodes, while the rate capability of these materials is relatively poor [2–4]. Besides, activated carbons (ACs) were usually used as the cathode for LICs. However, the specific capacity of ACs is always relatively low

( $\leq 50 \text{ mAh g}^{-1}$ ), owing to their ion adsorption/desorption mechanism. Thus, the mismatch of specific capacity between two electrodes, along with the sacrifice of the energy density, is a major problem without a doubt in LICs [5]. Moreover, the electrochemical kinetics of the anode material (battery-type) based on the redox reaction is much slower than that of cathode depending on the electric-double layer capacitive (EDLC) behavior, leading to unsatisfactory power density and kinetic mismatch between the cathode and anode. In this regard, it is of great significance to explore appropriate cathode and anode materials with matching internal dynamics and capacity for meeting high-performance requirements in LICs [6]. There are a lot of works focused on the improvement of electrochemical kinetics for anode materials to date. However, the cathode has gained little attention until now [7, 8]. In fact, the low specific capacity of the cathode is the most important bottleneck of LICs in practical applications.

Porous carbon, possessing large specific surface area (SSA), good conductivity, outstanding rate capability, and excellent cycle stability, is an ideal cathode material for LICs [9–13]. Notably, heteroatom doping (e.g., nitrogen [14–19], sulfur [20, 21], boron [22–24]) is usually employed to improve the electrochemical properties of carbon-based materials. Among them, nitrogen is considered to be the commonest doping element, owing to the approximate size relative to carbon atoms. Electrochemical reactive sites can be introduced and optimized by N-doped structure in a carbon skeleton, which enhances the surface-dominated charge storage [25–29]. For instance, Jia et al. synthesized a novel N/S co-doped carbon aerogel deriving from a methyl blue-doped polyaniline hydrogel [30]. The designed porous carbon exhibited an excellent electrochemical performance ( $300 \text{ F g}^{-1}$  at  $1 \text{ A g}^{-1}$ ). Recently, Xia et al. used N and B co-doped porous carbon nanofibers as an active material to assemble LIC, which showed a high energy density of  $104 \text{ Wh kg}^{-1}$  at a power density of  $22.5 \text{ kW kg}^{-1}$  with excellent cycling stability [24]. However, the optimal electrochemical performance cannot be achieved with heteroatom doping alone without structural design and regulation.

Actually, nanostructure engineering also plays an important role in electrochemical performance. In particular, the advantages of hierarchical porous carbon materials, including large surface area, relatively high electrical conductivity, reasonable pore size distribution, and excellent physiochemical

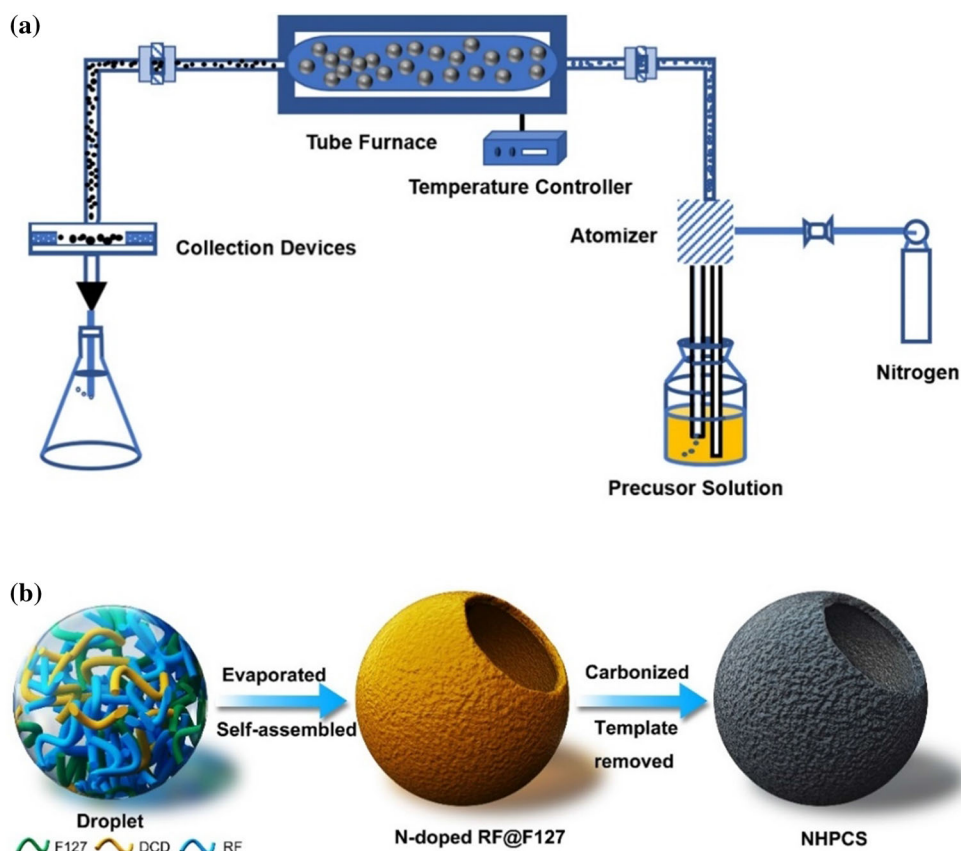
stability, greatly promote the ion/electron diffusion and optimize rate performance. Although some works on the hierarchical porous carbon have been reported previously, the synthesis processes are always complicated, expensive, and time-consuming [31, 32]. Taking this into account, the synthesis of functional porous carbon through a sustainable and efficient way without sacrificing properties is a great challenge until now.

Herein, we have synthesized the N-doped hierarchical porous carbon spheres (NHPCS) via a simple aerosol-spraying pyrolysis and following chemical activation process. Such facile and controllable procedure can prepare three-dimensional (3D) carbon material in a short minute based on the principle of self-assembly. The hierarchical structure and N-induced chemistry of NHPCS endow it with rapid kinetics and pseudocapacitive properties, which make it have better electrochemical performance than commercial AC cathode. With these merits, the as-fabricated LIC (NHPCS cathode and hard carbon anode) delivers a maximum energy density of  $151 \text{ Wh kg}^{-1}$  at a power density of  $215.5 \text{ W kg}^{-1}$ , and remains a high energy density of  $91 \text{ Wh kg}^{-1}$  even at a power density of  $10.7 \text{ kW kg}^{-1}$ . Furthermore, the capacity retention rate of the LIC is about 96.3% after 3000 cycles, showing great potential for the next-generation energy storage devices.

## Results and discussion

The preparation process of NHPCS was derived from the self-assembled aerosol-spraying device (Fig. 1a). Notably, such device can produce nano-sized spherical particles with narrow particle size distribution and without agglomeration in a relatively short period of time, which is very suitable for manufacturing desired electrode material in practical application [33]. The sample formation process is illustrated in Fig. 1b, and the concrete operation sequences are depicted in the experimental procedure (Supplementary Information). In brief, the phenolic resin (RF) was chosen as the carbon precursor, which can provide high yields and allow the production of porous carbon with a high surface area and a specific porosity [34, 35]. A self-assembly reaction was realized by introducing F127 (soft template) and dicyandiamide (DCD, nitrogen source) into RF to form a composite mesophase structure. Because of

**Figure 1** **a** Schematic diagram of the spray pyrolysis strategy, **b** schematic of the formation process of NHPCS.



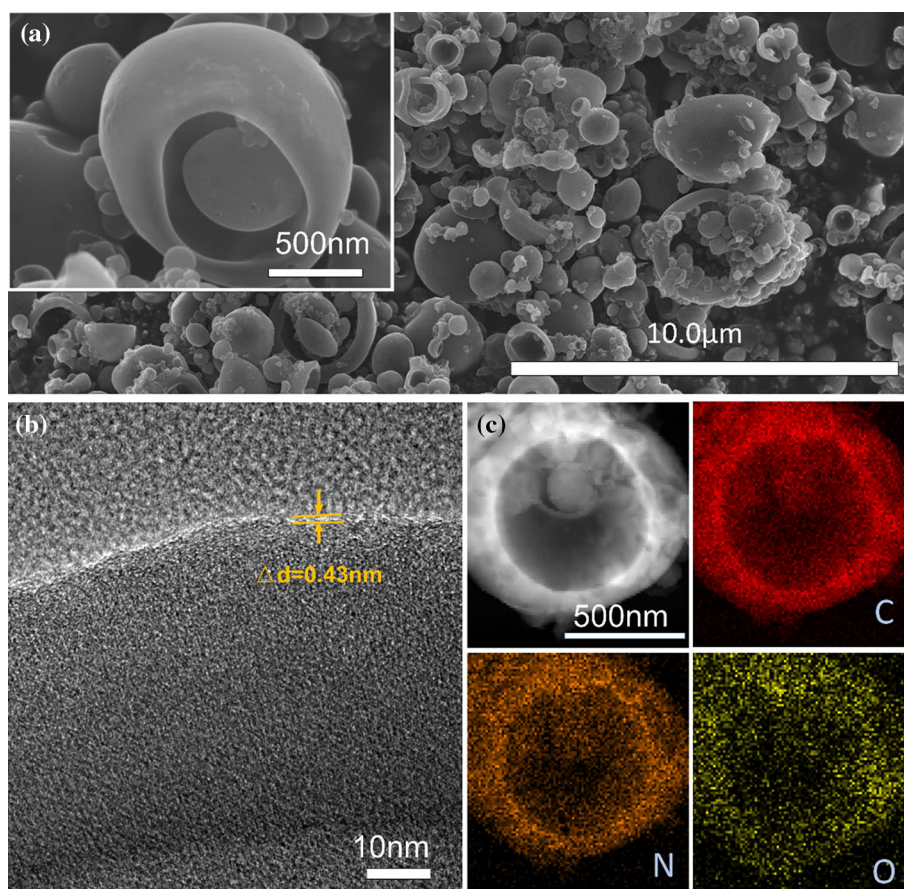
the strong interaction between F127 and RF, together with the high strength network skeleton of RF, stable special pores can be formed by the microphase pyrolysis of F127 micelles during the carbonization, which can realize the adjustable aperture and well satisfies the requirements of hierarchical porous materials.

The morphology structures of the obtained samples were studied by SEM and TEM. In particular, the as-obtained N-PCS (without activation) displays a spherical structure with a smooth surface (Fig. S1). It can be found that the HPCS (without nitrogen source introduced) also shows a large sphere structure with a diameter about 600–900 nm, but the surface is relatively rough (Fig. S2). Nevertheless, the morphology of NHPCS changes apparently with an increase in average particle size, which may be caused by the activation of KOH, as well as the addition of DCD (Fig. 2a). According to the high-resolution TEM (HRTEM) image of NHPCS, there are visible amorphous structure and abundant pores (Fig. 2b). Notably, the lattice spacing of the graphite plane (002) in NHPCS (0.43 nm) is larger than that of the typical graphite (0.34 nm), because the N-doping and violent

activation processes can enlarge the lattice spacing of carbon-based materials. To better comprehend the structural characteristics of NHPCS, it was further characterized by the high-angle annular dark-field (HAADF) image and corresponding energy-dispersive spectrometer (EDS) mapping. As shown in Fig. 2c, the compositional elements (C, O, N) overlap and distribute uniformly in NHPCS particles, implying the N element has been successfully doped into the carbon skeleton. In addition, the hollow structure of NHPCS remains intact after the hydrochloric acid etching and high-temperature carbonization processes.

X-ray photoelectron spectroscopy (XPS) measurement shows the existence of the N element (Fig. 3a), which is corresponding to the result of EDS mapping, while there are only two elements of C and O detected in HPCS. Based on the result of the XPS analysis, the corresponding content of nitrogen is 3.65 at.% in NHPCS, and other elements contents are summarized in Table. S1. The high-resolution C 1s peaks of NHPCS and HPCS play a leading role by the C=C at  $284.7 \pm 0.2$  eV, and the other weaker peaks are assigned to the C–O ( $285.2 \pm 0.2$  eV), C=O

**Figure 2** **a** SEM and **b** HRTEM images of NHPCS particles. **c** HAADF-STEM image of NHPCS, and corresponding to the mapping images of the C, N, and O elements.

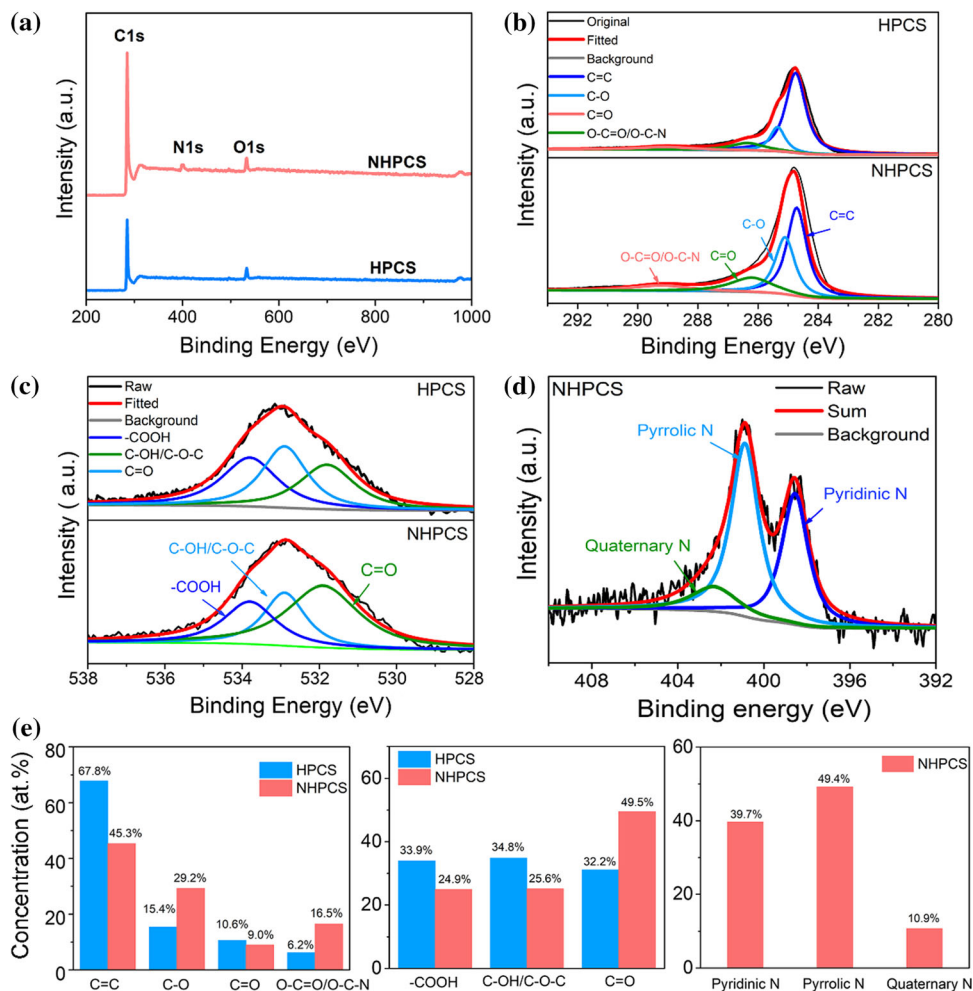


( $286.2 \pm 0.2$  eV), and  $\text{O-C=O/O-C-N}$  ( $289.2 \pm 0.2$  eV), respectively (Fig. 3b) [36, 37]. Among them, the peak area ratio of C–O bond and  $\text{O-C=O/O-C-N}$  bond in NHPCS and HPCS are significantly lower than other two peaks (Fig. 3e), which may be related to the KOH activation process [38]. Given in Fig. 3c and 3e, the high-resolution O 1s spectra of NHPCS and HPCS can be divided into the three components of  $-\text{COOH}$  ( $533.6 \pm 0.2$  eV),  $\text{C-OH/C-O-C}$  ( $532.9 \pm 0.2$  eV), and  $\text{C=O}$  ( $531.8 \pm 0.2$  eV). All the corresponding percentage of functional groups is similar in this material [39, 40]. In particular, the high-resolution N 1s spectra of NHPCS show the high density of pyridine-N ( $398.6 \pm 0.2$  eV) and pyrrolic-N ( $400.9 \pm 0.2$  eV) functional groups, while the quaternary-N ( $402.2 \pm 0.2$  eV) is the weakest (Fig. 3d, e) [41–45]. Among these N species, the pyridine-N and pyrrolic-N possess the remarkable electron donor characteristics and charge transfer ability, which can introduce additional pseudocapacitance contribution by causing the surface polarization of carbon skeleton, thereby boosting the specific capacity for carbon-

based materials [30]. Some pyridine-N atoms could be oxidized due to the activation reaction process between the carbon sheets with KOH at high temperature [46]. Besides, the quaternary-N is an integral part of the planar graphite carbon, which can enhance the electronic transmission throughout the carbon plane and improve electronic conductivity [22]. These results show that the capacitive charge storage capability of NHPCS is expected to boost, which is testified in the following discussion.

To further understand the phase composition and pore structure of NHPCS and HPCS, the XRD, Raman, and  $\text{N}_2$  adsorption/desorption tests were carried out. The crystal phase analyses of NHPCS and HPCS are shown in Fig. 4a. Both of them display two typical characteristic peaks of the graphitized carbon, corresponding to (002) and (100) reflection planes. It can be seen that the (002) plane of NHPCS exhibits a slight shift toward the low angle ( $22.1^\circ$ ), demonstrating that the lattice constant increases, and the nitrogen atoms are successfully incorporated into the carbon skeleton. Based on the Bragg equation ( $2d_{(002)}\sin\theta = \lambda$ ), the calculated value of  $d_{(002)}$  is

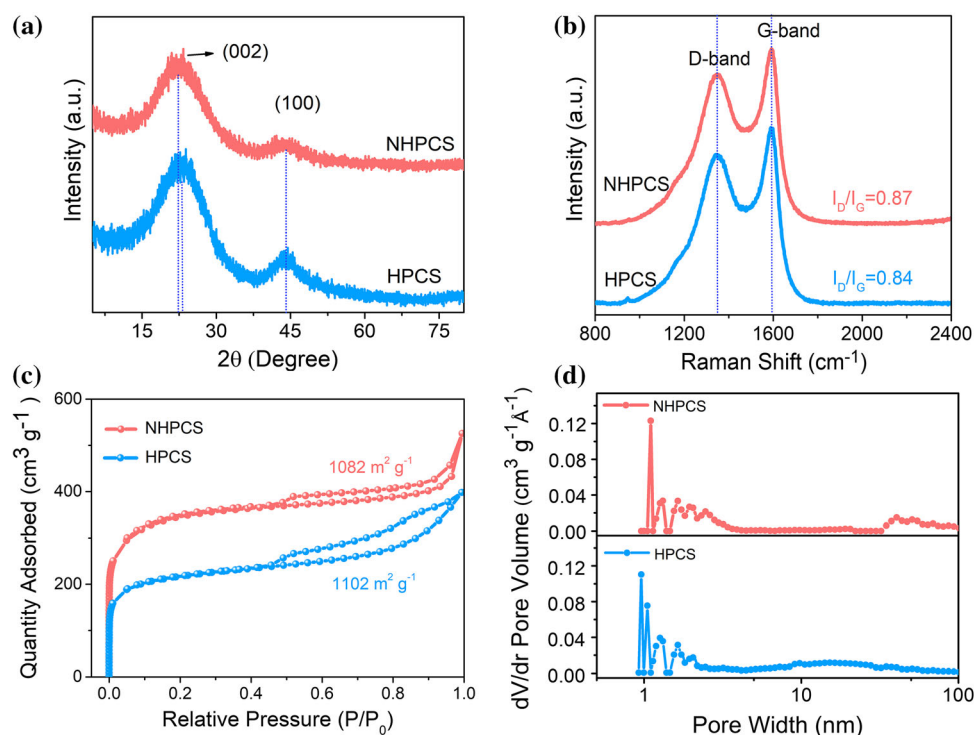
**Figure 3** a Overall XPS spectra of NHPCS and HPCS. High-resolution XPS spectra of b C 1s, c O 1s, and d N 1s for NHPCS and HPCS. e The contents of heteroatom species of the C, O, N elements.



0.40 nm, which is almost consistent with the HRTEM image measurement result, indicating the larger carbon layer spacing [47]. As shown in Fig. 4b, Raman spectra show that NHPCS and HPCS have a broad D band at  $1320\text{ cm}^{-1}$ , which corresponds to the defect site and the  $sp^3$  hybridized of carbon material. The G bands at  $1590\text{ cm}^{-1}$  can be attributed to the  $sp^2$  of the hexagonal lattice carbon [48]. Typically, the intensity ratio for D/G band ( $I_D/I_G$ ) is applied to judge the extent of graphitization and defect structure for carbon material. The  $I_D/I_G$  value of NHPCS (0.87) is relatively higher than HPCS (0.84), demonstrating that the nanostructure of NHPCS is more disordered after a high-performance N-doping. Therefore, more amorphous carbon structures with defects and active sites are generated in NHPCS (results obtained by XRD, Raman, and HRTEM), which shows promise to achieve an outstanding capacitive charge storage performance for cathode materials.

The specific surface area (SSA) and pore structure of the samples are explored by  $N_2$  adsorption isotherm. For N-PCS, the SSA is  $371\text{ m}^2\text{ g}^{-1}$ , which can be classified as type IV, suggesting the presence of mesopores in this sample (Fig. S3). This result is agreed with the using of F127 as a soft template, which plays an essential role in mesoporous formation. As shown in Fig. 4c, the corresponding SSA of HPCS and NHPCS is  $1102$  and  $1082\text{ m}^2\text{ g}^{-1}$ , displaying hybrid isotherm of typical I/IV types, respectively [49]. It is worth noting that the adsorption capacity increased obviously at low pressure, indicating the existence of micropores structure. The KOH activation can efficiently generate the microporous and improve the specific surface area for carbon-based materials. Meanwhile, the capillary condensation occurred at relative pressure between 0.5 and 1.0 which results in a hysteresis loop, suggesting the existence of mesopores in both HPCS and NHPCS. The pore size distribution is further

**Figure 4** **a** XRD and **b** Raman spectra of NHPCS and HPCS. **c** N<sub>2</sub> adsorption isotherms, and **d** pore-size distribution curves of HPCS and NHPCS.



calculated by the density functional theory (DFT) model (Fig. 4d and Fig. S3). In detail, the pore sizes of HPCS and NHPCS are mainly centered at 0.8–4 nm, and much smaller than N-HPCS (> 8.3 nm), which is due to the high-temperature pyrolysis and the activation of KOH ( $6 \text{ KOH} + \text{C} \rightarrow 2 \text{ K} + 3 \text{ H}_2 + 2 \text{ K}_2\text{CO}_3$ ). Among them, the reaction products (such as bubbles generated in the activation process) play the part of exploiting porous templates [47]. Moreover, HPCS also exhibits the minimum micropore volume of  $0.40 \text{ m}^2 \text{ g}^{-1}$ , which can be calculated from t-plot method, and the NHPCS is  $0.43 \text{ m}^2 \text{ g}^{-1}$ . More details of SSA and pore parameters can be found in Table S2. Combined with the above physical characterization results, both of NHPCS and HPCS are equipped with a relatively large interlayer spacing, a high SSA and low average pore sizes distribution, which would promote electrolyte ion (such as  $\text{PF}_6^-$ ) diffusion into the interlayer space and hierarchical pores, and thus effectively improve the specific capacity and rate capability. As shown in Fig. S4, the NHPCS electrode has good penetration characteristics for organic electrolyte (1 M  $\text{LiPF}_6$  in EC:DMC:DEC). The contact angle is  $13.3^\circ$  after dropping the electrolyte for 3 s, while the soak of HPCS electrode is relatively poor with the contact angle of  $22.4^\circ$ . This result shows

that N-doping can effectively improve the wettability of the NHPCS electrode.

With the advantages of high SSA, hierarchical porous structure, and good wettability, NHPCS is expected to become an ideal cathode material for the preparation of carbon-based LICs. The energy storage behaviors of NHPCS and HPCS cathodes were systematically studied in half-cell configuration with lithium foil as the counter/reference electrode. To demonstrate the merit of the unique structure and N-doping in NHPCS, the electrochemical properties of commercial AC and N-PCC were carried out under the same conditions. The cyclic voltammetry (CV) curves of NHPCS and HPCS at a scan rate of  $100 \text{ mV s}^{-1}$  are depicted in Fig. 5a with the potential range of 2.0–4.3 V. HPCS shows a regular rectangular shape, whereas the NHPCS exhibits a nearly quasi-rectangle form with a small hump. This suggests the co-existence of both EDLC and pseudocapacitive procedures in NHPCS. To our knowledge, the typical contribution of EDLC can be ascribed to the physical adsorption/desorption of  $\text{PF}_6^-$  on the carbon surface, while the pseudocapacitive processes are generated by the interaction between the electrolyte ions and the heteroatoms-containing functional groups [50–52]. Compared with the rectangular-like CV curves of HPCS (only with O doping) in Fig. S5, the

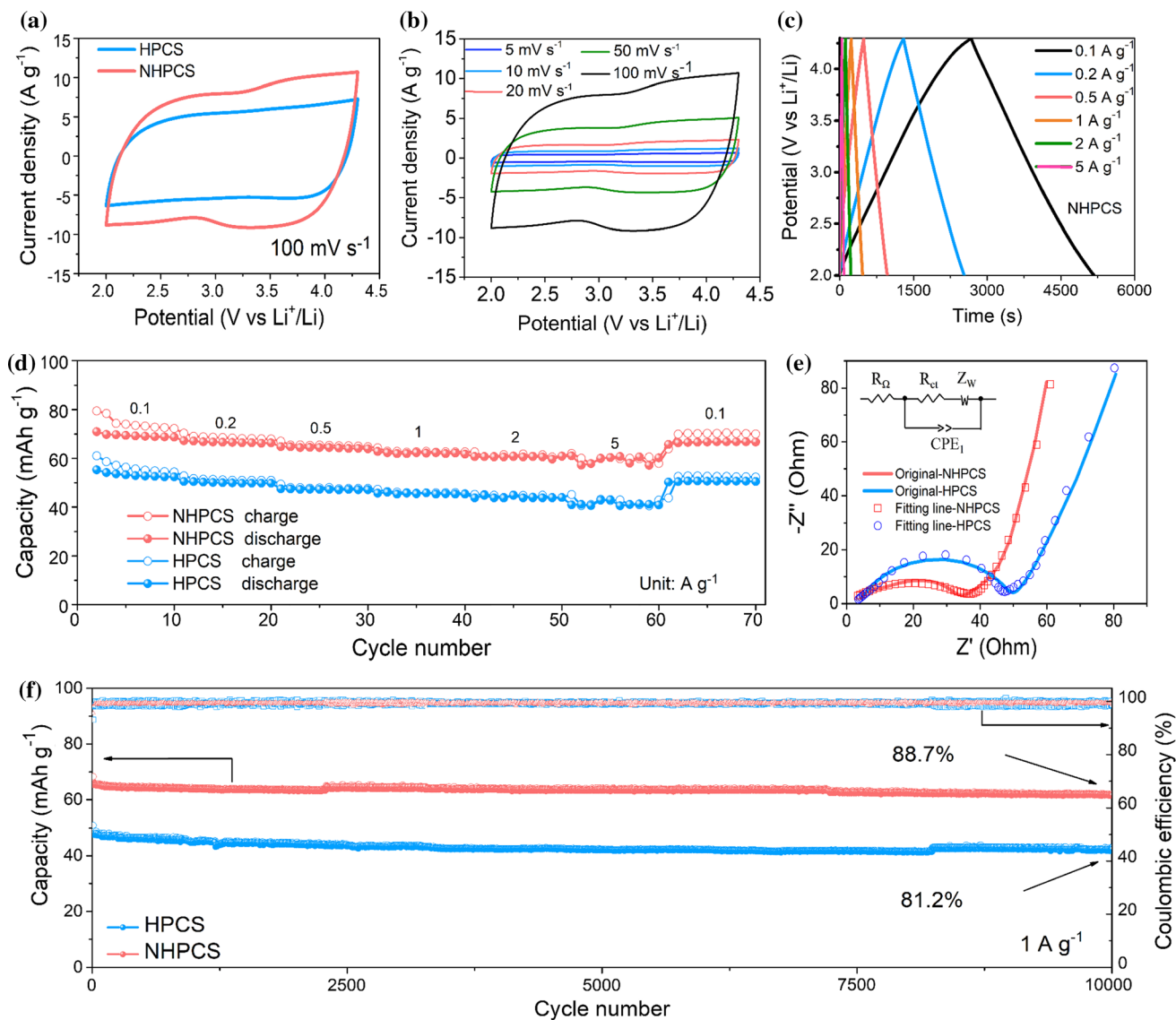


**Figure 5** **a** CV curves of NHPCS and HPCS at the same scan rate of  $100 \text{ mV s}^{-1}$ . **b** CV curves of NHPCS with various scan rates. **c** GCD curves at different current densities ( $0.1\text{--}5 \text{ A g}^{-1}$ ). **d** Rate

capabilities of NHPCS and HPCS. **e** Nyquist plots of NHPCS and HPCS electrodes. **f** Cycling performances of NHPCS and HPCS at a current density of  $1 \text{ A g}^{-1}$ .

NHPCS exhibits a larger enclosed area at each scan rate along with the combined energy storage behaviors, which further indicates the great improvement in electrochemical property based on the co-doping of N and O elements. Furthermore, the CV curves of NHPCS and HPCS remain quasi-rectangle shapes without serious deformation even at the scan rate up to  $100 \text{ mV s}^{-1}$ , implying the incredibly tiny electrode polarization as well as an excellent rate capability (Fig. 5b and Fig. S5). As shown in Fig. 5c and Fig. S6, the galvanostatic charge–discharge (GCD) profiles of NHPCS and HPCS under different current densities (from  $0.1$  to  $5 \text{ A g}^{-1}$ ) are presented. All curves exhibit

similar linear shapes, demonstrating the good reversibility and capacitive behavior. Among them, the GCD curves of NHPCS hold the longer discharge time, implying the higher specific capacities at different current densities. Moreover, the comparison of the rate capability for NHPCS, HPCS, N-PCS, and AC at various current densities is given in Fig. 5d and Fig. S7. In particular, the NHPCS achieves a specific capacity of  $74 \text{ mAh g}^{-1}$  at  $0.1 \text{ A g}^{-1}$ , which is higher than that of other as-prepared materials, such as HPCS ( $57 \text{ mAh g}^{-1}$ ), N-PCS ( $30 \text{ mAh g}^{-1}$ ), and AC ( $49 \text{ mAh g}^{-1}$ ), respectively. Even be subjected to a high rate of  $5 \text{ A g}^{-1}$ , the specific capacity retention of



NHPCS is 86.5%, and that of N-PCS is 78.3%. However, the HPCS and AC are dropped to only 73.6% and 72.1% at the same current density, respectively. It should be noted that the rate performance and specific capacity of NHPCS are beyond the HPCS, N-PCS, and AC. The electrochemical impedance spectroscopy (EIS) of NHPCS and HPCS is also tested and fitted (Fig. 5e). The first intercept of the real axis ( $Z'$ ) represents the ohmic resistance ( $R_s$ ), while the charge transfer resistance effect ( $R_{ct}$ ) is reflected by the semicircle at high frequency. Based on the equivalent circuits, the NHPCS electrode exhibits the minimum  $R_s$  (3.42  $\Omega$ ) and  $R_{ct}$  (38.33  $\Omega$ ), manifesting the better conductivity of NHPCS framework and more effective electrolyte ion diffusion at the electrode surface. In addition, Nyquist plots of NHPCS and HPCS show a relatively vertical curve at low frequency, indicating the remarkable capacitive behavior. In view of the similar pore structure and the same mass loading for NHPCS and HPCS electrodes, the optimized electrode kinetics of NHPCS electrode may be originated from good wettability, which can reduce the interface impedance, and thus, further boost rate performance. As depicted in Fig. 5f, NHPCS electrode exhibits the capacity retention up to 88.7% over 10,000 cycles at a current density of 1 A  $g^{-1}$ , which is superior to that of HPCS (81.2%). Notably, the cyclic performance of the NHPCS electrode is also much better than that of most porous carbon materials and commercial AC [24, 50]. These remarkable electrochemical properties of NHPCS make it become one of the promising cathode materials for high-performance LICs.

It is of great significance for a high capacity electrode to investigate the correlation between pore structure and specific capacity. In general, the

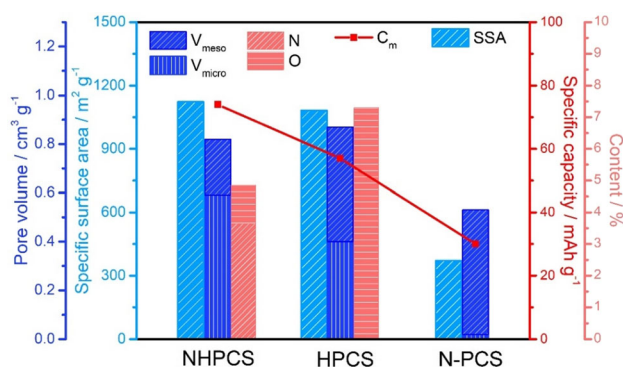


**Figure 6** The relationship among the specific capacity of NHPCS and HPCS between the microstructure and heteroatomic content.

capacity of carbon-based porous materials is positively related to the specific surface area, but this description is not accurate, especially at the circumstances of heteroatom-doping [47]. As shown in Fig. 6, the SSA of NHPCS is 1082  $m^2 g^{-1}$  lower than that of HPCS (1102  $m^2 g^{-1}$ ); however, the specific capacity of NHPCS is much higher than HPCS. This may be related to the solvated dimensions of  $PF_6^-$  ions in the electrolyte, and its diameter is about 0.9 nm [53]. Based on the results of nitrogen adsorption/desorption tests (Table. S2), the lowest average micropore width of HPCS is approximately 0.50 nm, which is far less than the size of solvated  $PF_6^-$  ions, while the NHPCS is 0.76 nm, closing to the diameter of solvated  $PF_6^-$ . Therefore, some micropores in HPCS are ineffective and the electrochemically effective SSA is reduced, which is the one of the reasons for poor capacitive charge storage of the HPCS. Compared with N-PCS, the micropore volume and total pore volume of NHPCS and HPCS are increased. Furthermore, the electronic natures of the N-doped carbon material can be changed, which is ascribed to the N electronic configuration, making it more beneficial to attract ions in the electrolyte [54]. The capacitance property rises greatly by introducing N-doping, which is further proved via constructing EDLC devices (Fig. S8 and Fig. S9). Therefore, the excellent specific capacity of NHPCS is bound up with the internal synergy among high effective SSA, high porosity, and heteroatom doping.

To explore the practical applications, the LIC was prepared using the NHPCS or HPCS as cathode, and commercial hard carbon (HC) (provided by KUR-EHA Co., Ltd, more electrochemical characterizations are shown in Fig. S10 and Fig. S11) as anode, respectively. Based on the quality matching principles, the mass ratio of cathode and anode is determined to be 3:1 [38, 55]. The specific working mechanism of the fabricated LIC (NHPCS//HC) during charge–discharge cycles is illustrated in Fig. 7a, where  $Li^+$  inserts the interlayer of the HC anode; meantime,  $PF_6^-$  ion accumulates on the N-doped carbon pore and surface of NHPCS cathode [56]. The CV profiles of LIC (NHPCS//HC) are quasi-rectangular at the low scan rate (Fig. 7b). When the scan rate increased from 5 to 50  $mV s^{-1}$ , the shape of the curves remains unchanged with a high cell voltage of 0.01–4.3 V, implying its outstanding reversibility and excellent rate capability. Notably, the CV curve shapes of the as-assembled device show

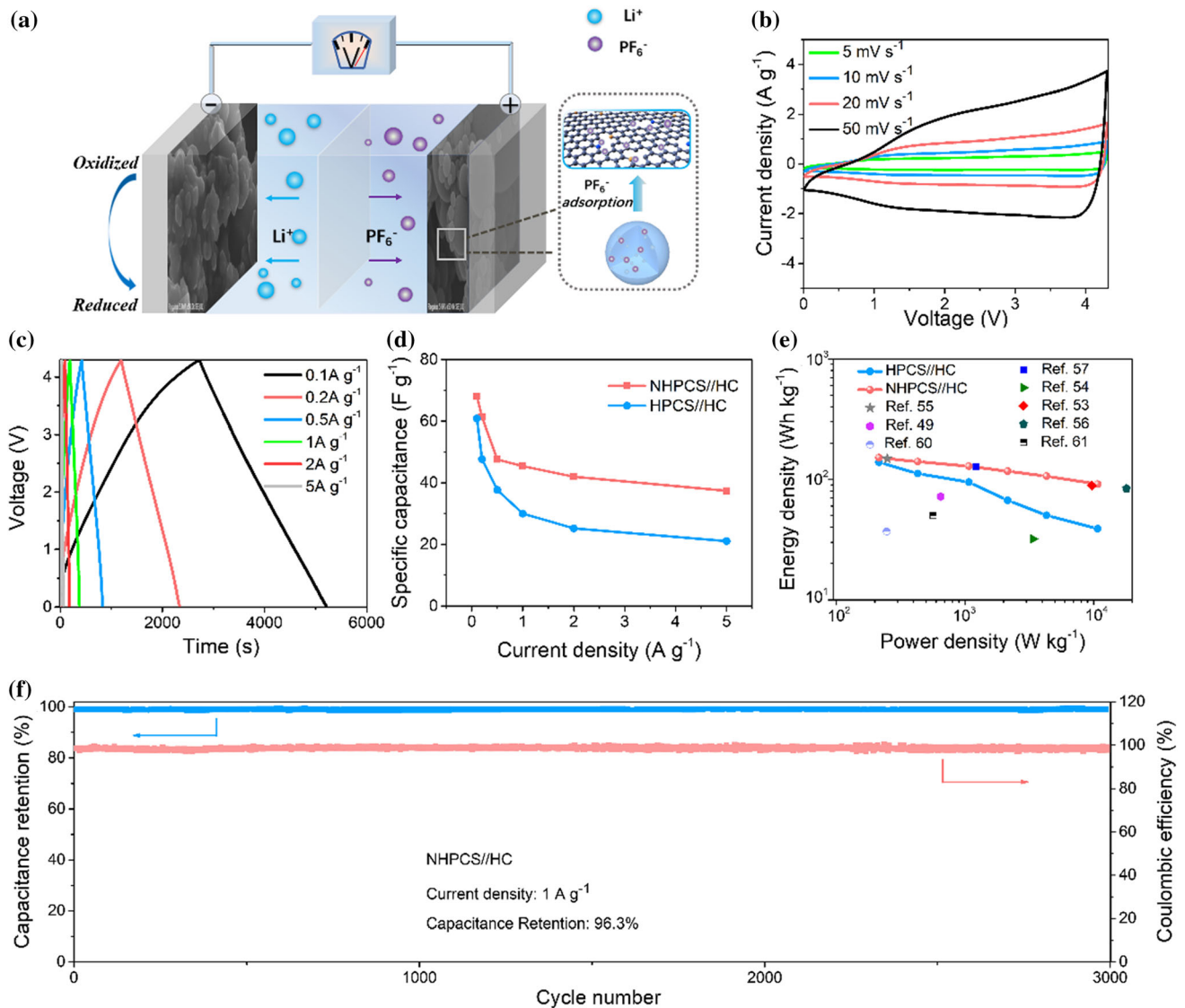


**Figure 7** a Schematic illustration of the charge–discharge storage mechanisms of as-assembled LIC (NHPCS//HC) device. b CV profiles of LIC at various scan rates in the voltage range of 0.01–4.3 V. c GCD curves of LIC at different current densities.

a difference compared with the EDLC, because of the “synergistic effect” between the cathode and anode electrodes in LIC, in which the adsorption/desorption mechanism of the cathode, and the redox reaction mechanism of the anode are combined. GCD profiles of LIC (NHPCS//HC and HPCS//HC) contain a highly symmetrical and linear slope (Fig. 7c and Fig. S13). Besides, it has a negligible voltage drop in the current density range of 0.1–5  $A g^{-1}$ , indicating the small electrode polarization of the device even at high current density. In particular, the corresponding specific capacitance can achieve the values of 68, 61.3,

d The specific capacitances of LICs (NHPCS//HC and HPCS//HC) at different current densities. e Ragone plots in comparison with other literatures. f Cycle life of LIC at a current density of 1  $A g^{-1}$ .

47.6, 45.4, 42.0, and 37.4  $F g^{-1}$  at 0.1, 0.2, 0.5, 1, 2, and 5  $A g^{-1}$  for the as-assembled LIC (NHPCS//HC), whereas the other fabricated LIC (HPCS//HC) acquires only 60.8, 47.7, 36.7, 29.7, 25.2, and 21  $F g^{-1}$  at 0.1, 0.2, 0.5, 1, 2, and 5  $A g^{-1}$ , respectively (Fig. 7d).

According to a total mass of cathode and anode, the specific energy and specific power were calculated. As expected, the LIC (NHPCS//HC) achieves a remarkable energy density of up to 151  $Wh kg^{-1}$  at the power density of 215.5  $W kg^{-1}$ . Notably, it can still remain 91  $Wh kg^{-1}$  even at an extremely high power density of 10.7  $kW kg^{-1}$  (Fig. 7e). Moreover,

the LIC (NHPCS//HC) delivers outstanding capacity retention of 96.3% after 3000 cycles at a current density of  $1 \text{ A g}^{-1}$  (Fig. 7f), implying extraordinary cycle stability. The prominent energy and power density of LIC (NHPCS//HC) are also the first-rate level compared with previously reported LIC systems, for instance, CNS//MnO@CNS systems [56], AC//HC [57], AC//LTO [3, 58], AC//B-Si@SiO<sub>2</sub>@C [59], HNVNB//PHNCNB [50], 3D graphene//Fe<sub>3</sub>O<sub>4</sub>@graphene [35], CSCs//CSCs [60], NBC//LiMn<sub>2</sub>O<sub>4</sub> [61]. As shown in Table. S3, the electrochemical parameters of our assembled LIC (NHPCS//HC) are more competitive relative to the reported carbon-based LICs, portending promising practical application and prospects.

## Conclusions

In conclusion, N-doped hierarchical porous carbon spheres (NHPCS) have been prepared by a larger-scale spray pyrolysis strategy. Owing to their hierarchical porous structure and suitable N-doped level, the NHPCS as a cathode achieves a high specific capacity of  $74 \text{ mAh g}^{-1}$  at a current density of  $0.1 \text{ A g}^{-1}$ , and remains with  $64 \text{ mAh g}^{-1}$  even at a high current density of  $5 \text{ A g}^{-1}$ . In addition, the capacity retention rate is high up to 88.7% after 10,000 cycles, which is only 0.077% capacity decay per cycle. The N-doping can not only improve the wettability, but also enhance the electrochemical kinetics. Thus, the NHPCS acquires a better electrochemical performance, when used as an electrode material for EDLC and LIC. The as-fabricated LIC (NHPCS//HC) exhibits a maximum energy density of  $151 \text{ Wh kg}^{-1}$  at the power density of  $215.5 \text{ W kg}^{-1}$ . The energy density can still retain  $91 \text{ Wh kg}^{-1}$  at a high power density of  $10.7 \text{ kW kg}^{-1}$ . Furthermore, the retention rate of capacity is 96.3% after 3000 cycles, providing an attractive hybrid energy storage device for the practical application.

## Experiment section

Experimental details are available from the supplementary material.

## Acknowledgements

This work was financially supported by the National Natural Science Foundation of China (U1802256, 51672128, 21773118, 21875107), the Key Research and Development Program in Jiangsu Province (BE2018122) and Project Funded by the Priority Academic Program Development of Jiangsu Higher Education Institutions (PAPD). Mr. Ziqian Yang would like to acknowledge the financial support from the Undergraduate Innovation and Entrepreneurship Training Program in NUAA (2019CX00602).

## Compliance with ethical standards

**Conflict of interest** The authors declare no conflict of interest.

**Electronic supplementary material:** The online version of this article (<https://doi.org/10.1007/s10853-020-04955-2>) contains supplementary material, which is available to authorized users.

## References

- [1] Simon P, Gogotsi Y (2008) Materials for electrochemical capacitors. *Nat Mater* 7:320–329
- [2] Shen L, Lv H, Chen S, Kopold P, Aken PA, Wu X, Maier J, Yu Y (2017) Peapod-like Li<sub>3</sub>VO<sub>4</sub>/N-doped carbon nanowires with pseudocapacitive properties as advanced materials for high-energy lithium-ion capacitors. *Adv Mater* 29:1700142
- [3] Ye L, Liang Q, Lei Y, Yu X, Han C, Shen W, Huang ZH, Kang F, Yang QH (2015) A high performance Li-ion capacitor constructed with Li<sub>4</sub>Ti<sub>5</sub>O<sub>12</sub>/C hybrid and porous graphene macroform. *J Power Sources* 282:174–178
- [4] Ma C, Zhao Y, Li J, Song Y, Shi J, Guo Q, Liu L (2013) Synthesis and electrochemical properties of artificial graphite as an anode for high-performance lithium-ion batteries. *Carbon* 64:553–556
- [5] Kim J-H, Kim J-S, Lim Y-G, Lee J-G, Kim Y-J (2011) Effect of carbon types on the electrochemical properties of negative electrodes for Li-ion capacitors. *J Power Sour* 196:10490–10495
- [6] Shao Y, El-Kady MF, Sun J, Li Y, Zhang Q, Zhu M, Wang H, Dunn B, Kaner RB (2018) Design and mechanisms of asymmetric supercapacitors. *Chem Rev* 118:9233–9280
- [7] Chen Z, Li H, Lu X, Wu L, Jiang J, Jiang S, Wang J, Dou H, Zhang X (2018) Nitrogenated urchin-like Nb<sub>2</sub>O<sub>5</sub>

- microspheres with extraordinary pseudocapacitive properties for lithium-ion capacitors. *ChemElectroChem* 5:1516–1524
- [8] Jiang J, Zhang Y, An Y, Wu L, Zhu Q, Dou H, Zhang X (2019) Engineering ultrathin MoS<sub>2</sub> nanosheets anchored on N-Doped carbon microspheres with pseudocapacitive properties for high-performance lithium-ion capacitors. *Small Methods* 3:1900081
- [9] Gogotsi Y, Nikitin A, Ye H, Zhou W, Fischer JE, Yi B, Foley H, Barsoum MW (2012) Nanoporous carbide-derived carbon with tunable pore size. *Nat Mater* 2:591–594
- [10] Largeot C, Portet C, Chmiola J, Taberna PL, Gogotsi Y, Simon P (2008) Relation between the ion size and pore size for an electric double-layer capacitor. *J Am Chem Soc* 130:2730–2731
- [11] Wang J, Shen L, Nie P, Yun X, Xu Y, Dou H, Zhang X (2015) N-doped carbon foam based three-dimensional electrode architectures and asymmetric supercapacitors. *J Mater Chem A* 3:2853–2860
- [12] Wang R, Lang J, Zhang P, Lin Z, Yan X (2015) Fast and large lithium storage in 3D porous VN nanowires-graphene composite as a superior anode toward high-performance hybrid supercapacitors. *Adv Funct Mater* 25:2270–2278
- [13] Wang J, Kim J, Ding B, Kim JH, Malgras V, Young C, Yamauchi Y (2019) Ultra-thin, highly graphitized carbon nanosheets into three-dimensional interconnected framework utilizing a ball mill mixing of precursors. *Chem Eng J* 374:1214–1220
- [14] Li Z, Xu Z, Tan X, Wang H, Holt C, Stephenson T, Olsen B, Mitlin D (2013) Mesoporous nitrogen-rich carbons derived from protein for ultra-high capacity battery anodes and supercapacitors. *Energy Environ Sci* 6:871–878
- [15] Wei J, Zhou D, Sun Z, Deng Y, Xia Y, Zhao D (2012) A controllable synthesis of rich nitrogen-doped ordered mesoporous carbon for CO<sub>2</sub> capture and supercapacitors. *Adv Funct Mater* 23:2322–2328
- [16] Zheng F, Yang Y, Chen Q (2014) High lithium anodic performance of highly nitrogen-doped porous carbon prepared from a metal-organic framework. *Nat Commun* 5:5261
- [17] Wang Y, Wang C, Guo H, Wang Y, Huang Z (2017) A nitrogen-doped three-dimensional carbon framework for high performance sodium ion batteries. *RSC Adv* 7:1588–1592
- [18] Wang H, Zhang Y, Ang H, Zhang Y, Tan HT, Zhang Y, Guo Y, Franklin JB, Wu XL, Srinivasan M, Fan HJ, Yan Q (2016) A high-energy lithium-ion capacitor by integration of a 3D interconnected titanium carbide nanoparticle chain anode with a pyridine-derived porous nitrogen-doped carbon cathode. *Adv Funct Mater* 26:3082–3093
- [19] Du J, Liu L, Wu H, Chen A (2019) N-doped yolk-shell carbon nanotube composite for enhanced electrochemical performance in a supercapacitor. *Nanoscale* 11:22796–22803
- [20] Li Y, Wang G, Wei T, Fan Z, Yan P (2016) Nitrogen and sulfur co-doped porous carbon nanosheets derived from willow catkin for supercapacitors. *Nano Energy* 19:165–175
- [21] Yang C, Li W, Yang Z, Gu L, Yu Y (2015) Nanoconfined antimony in sulfur and nitrogen co-doped three-dimensionally (3D) interconnected macroporous carbon for high-performance sodium-ion batteries. *Nano Energy* 18:12–19
- [22] Jiang J, Nie P, Fang S, Zhang Y, An Y, Fu R, Dou H, Zhang X (2018) Boron and nitrogen dual-doped carbon as a novel cathode for high performance hybrid ion capacitors. *Chin Chem Lett* 29:624–628
- [23] Zhu J, He C, Li Y, Kang S, Shen PK (2013) One-step synthesis of boron and nitrogen-dual-self-doped graphene sheets as non-metal catalysts for oxygen reduction reaction. *J Mater Chem A* 1:14700–14705
- [24] Xia Q, Yang H, Wang M, Yang M, Guo Q, Wan L, Xia H, Yu Y (2017) High energy and high power lithium-ion capacitors based on boron and nitrogen dual-doped 3D carbon nanofibers as both cathode and anode. *Adv Energy Mater* 7:1701336
- [25] Beguin F, Szostak K, Lota G, Frackowiak E (2005) A self-supporting electrode for supercapacitors prepared by one-step pyrolysis of carbon nanotube/polyacrylonitrile blends. *Adv Mater* 17:2380–2384
- [26] Chen Y, Zhang X, Zhang D, Yu P, Ma Y (2011) High performance supercapacitors based on reduced graphene oxide in aqueous and ionic liquid electrolytes. *Carbon* 49:573–580
- [27] Jeong HM, Lee JW, Shin WH, Choi YJ, Shin HJ, Kang JK, Choi JW (2011) Nitrogen-doped graphene for high-performance ultracapacitors and the importance of nitrogen-doped sites at basal planes. *Nano Lett* 11:2472–2477
- [28] Li B, Dai F, Xiao Q, Yang L, Shen J, Zhang C, Cai M (2016) Nitrogen-doped activated carbon for a high energy hybrid supercapacitor. *Energy Environ Sci* 9:102–106
- [29] Raymundo-Pinero E, Cadek M, Beguin F (2009) Tuning carbon materials for supercapacitors by direct pyrolysis of seaweeds. *Adv Funct Mater* 19:1032–1039
- [30] Jia Q, Yang C, Pan Q, Xin Y, Xu F, Qi W, Wei H, Yang S, Zhou C, Hu N, Cao B (2020) High-voltage aqueous asymmetric pseudocapacitors based on methyl blue-doped polyaniline hydrogels and the derived N/S-codoped carbon aerogels. *Chem Eng J* 383:123153
- [31] Wang C, Wang F, Liu Z, Zhao Y, Liu Y, Yue Q, Zhu H, Deng Y, Wu Y, Zhao D (2017) N-doped carbon hollow microspheres for metal-free quasi-solid-state full sodium-ion capacitors. *Nano Energy* 41:674–680

- [32] Qiu D, Gao A, Xie Z, Zheng L, Kang C, Li Y, Guo N, Li M, Wang F, Yang R (2018) Homologous hierarchical porous hollow carbon spheres anode and bowls cathode enabling high-energy sodium-ion hybrid capacitors. *ACS Appl Mater Interfaces* 10:44483–44493
- [33] Leng J, Wang Z, Wang J, Wu HH, Yan G, Li X, Guo H, Liu Y, Zhang Q, Guo Z (2019) Advances in nanostructures fabricated via spray pyrolysis and their applications in energy storage and conversion. *Chem Soc Rev* 48:3015–3072
- [34] Moreno-Fernández G, Gómez-Urbano JL, Enterría M, Rojo T, Carriazo D (2019) Flat-shaped carbon–graphene micro-composites as electrodes for high energy supercapacitors. *J Mater Chem A* 7:14646–14655
- [35] Zhang F, Zhang T, Yang X, Zhang L, Leng K, Huang Y, Chen Y (2013) A high-performance supercapacitor-battery hybrid energy storage device based on graphene-enhanced electrode materials with ultrahigh energy density. *Energy Environ Sci* 6:1623–1632
- [36] Chen CM, Zhang Q, Yang MG, Huang CH, Yang YG, Wang MZ (2012) Structural evolution during annealing of thermally reduced graphene nanosheets for application in supercapacitors. *Carbon* 50:3572–3584
- [37] Li Z, Xu Z, Wang H, Ding J, Zahiri B, Holt CMB, Tan X, Mitlin D (2014) Colossal pseudocapacitance in a high functionality-high surface area carbon anode doubles the energy of an asymmetric supercapacitor. *Energy Environ Sci* 7:1708–1718
- [38] Jiang J, Yuan J, Nie P, Zhu Q, Chen C, He W, Zhang T, Dou H, Zhang X (2020) Hierarchical N-doped hollow carbon microspheres as advanced materials for high-performance lithium-ion capacitors. *J Mater Chem A* 8:3956–3966
- [39] Wang C, Wang X, Lu H, Li H, Zhao XS (2018) Cellulose-derived hierarchical porous carbon for high-performance flexible supercapacitors. *Carbon* 140:139–147
- [40] Xu SW, Zhao YQ, Xu YX, Chen QH, Zhang GQ, Xu QQ, Zhao DD, Zhang X, Xu CL (2018) Heteroatom doped porous carbon sheets derived from protein-rich wheat gluten for supercapacitors: the synergistic effect of pore properties and heteroatom on the electrochemical performance in different electrolytes. *J Power Source* 401:375–385
- [41] Li Z, Cao L, Chen W, Huang Z, Liu H (2019) Mesh-like carbon nanosheets with high-level nitrogen doping for high-energy dual-carbon lithium-ion capacitors. *Small* 15:1805173
- [42] Ania CO, Khomeiko V, Raymundo-Pinero E, Parra JB, Beguin F (2007) The large electrochemical capacitance of microporous doped carbon obtained by using a zeolite template. *Adv Funct Mater* 17:1828–1836
- [43] Pandolfo AG, Hollenkamp AF (2006) Carbon properties and their role in supercapacitors. *J Power Sources* 157:11–27
- [44] Silva R, Voiry D, Chhowalla M, Asefa T (2013) Efficient metal-free electrocatalysts for oxygen reduction: polyaniline-derived N- and O-doped mesoporous carbons. *J Am Chem Soc* 135:7823–7826
- [45] Biniaka S, Szymańska G, Siedlewska J, Świątkowski A (1997) The characterization of activated carbons with oxygen and nitrogen surface groups. *Carbon* 35:1799–1810
- [46] Li C, Zhang X, Wang K, Sun X, Ma Y (2018) High-power and long-life lithium-ion capacitors constructed from N-doped hierarchical carbon nanolayer cathode and mesoporous graphene anode. *Carbon* 140:237–248
- [47] Li Z, Mi H, Bai Z, Ji C, Sun L, Gao S, Qiu J (2019) Sustainable biowaste strategy to fabricate dual-doped carbon frameworks with remarkable performance for flexible solid-state supercapacitors. *J Power Sources* 418:112–121
- [48] Li Z, Gao S, Mi H, Lei C, Ji C, Xie Z, Yu C, Qiu J (2019) High-energy quasi-solid-state supercapacitors enabled by carbon nanofoam from biowaste and high-voltage inorganic gel electrolyte. *Carbon* 149:273–280
- [49] Li Z, Chen N, Mi H, Ma J, Xie Y, Qiu J (2017) Hierarchical hybrids integrated by dual polypyrrole-based porous carbons for enhanced capacitive performance. *Chemistry* 23:13474–13481
- [50] Liang T, Wang H, Fei R, Wang R, He B, Gong Y, Yan C (2019) A high-power lithium-ion hybrid capacitor based on a hollow N-doped carbon nanobox anode and its porous analogue cathode. *Nanoscale* 11:20715–20724
- [51] Sun F, Liu X, Wu HB, Wang L, Gao J, Li H, Lu Y (2018) In situ high-level nitrogen doping into carbon nanospheres and boosting of capacitive charge storage in both anode and cathode for a high-energy 4.5 V full-carbon lithium-ion capacitor. *Nano Lett* 18:3368–3376
- [52] Jiang YQ, Liu JP (2019) Definitions of pseudocapacitive materials: a brief review. *Energy Environ Mater* 2:30–37
- [53] Aref A, Chen SW, Rajagopalan R, Randall C (2019) Bimodal porous carbon cathode and prelithiated coalesced carbon anode for ultrahigh power energy efficient lithium ion capacitors. *Carbon* 152:89–97
- [54] Sun L, Zhou H, Li L, Yao Y, Qu H, Zhang C, Liu S, Zhou Y (2017) Double soft-template synthesis of nitrogen/sulfur-codoped hierarchically porous carbon materials derived from protic ionic liquid for supercapacitor. *ACS Appl Mater Interfaces* 9:26088–26095
- [55] Jiang J, Zhang Y, Li Z, An Y, Zhu Q, Xu Y, Zang S, Dou H, Zhang X (2020) Defect-rich and N-doped hard carbon as a sustainable anode for high-energy lithium-ion capacitors. *J Colloid Interface Sci* 567:75–83

- [56] Wang H, Xu Z, Li Z, Cui K, Ding J, Kohandehghan A, Tan X, Zahiri B, Olsen BC, Holt CMB, Mitlin D (2014) Hybrid device employing three-dimensional arrays of MnO in carbon nanosheets bridges battery–supercapacitor divide. *Nano Lett* 14:1987–1994
- [57] Zhang J, Liu X, Wang J, Shi J, Shi Z (2016) Different types of pre-lithiated hard carbon as negative electrode material for lithium-ion capacitors. *Electrochim Acta* 187:134–142
- [58] Wang G, Lu C, Zhang X, Wan B, Liu H, Xia M, Gou H, Xin G, Lian J, Zhang Y (2017) Toward ultrafast lithium ion capacitors: a novel atomic layer deposition seeded preparation of  $\text{Li}_4\text{Ti}_5\text{O}_{12}$ /graphene anode. *Nano Energy* 36:46–57
- [59] Yi R, Chen S, Song J, Gordin ML, Manivannan A, Wang D (2014) High-performance hybrid supercapacitor enabled by a high-rate Si-based anode. *Adv Funct Mater* 24:7433–7439
- [60] Li CY, Wu WZ, Wang P, Zhou WB, Wang J, Chen YH, Fu LJ, Zhu YS, Wu YP, Huang W (2019) Fabricating an aqueous symmetric supercapacitor with a stable high working voltage of 2 V by using an alkaline-acidic electrolyte. *Adv Sci* 6:1801665
- [61] Li CY, Wu WZ, Zhang SS, He L, Zhu YS, Wang J, Fu LJ, Chen YH, Wu YP, Huang W (2019) A high-voltage aqueous lithium ion capacitor with high energy density from an alkaline–neutral electrolyte. *J Mater Chem A* 7:4110–4118

**Publisher's Note** Springer Nature remains neutral with regard to jurisdictional claims in published maps and institutional affiliations.